Developmental Cell
Article

Global Analysis of the Meiotic Crossover Landscape

Stacy Y. Chen,[1] Tomomi Tsubouchi,[2,7] Beth Rockmill,[2,3] Jay S. Sandler,[1] Daniel R. Richards,[4] Gerben Vader,[5] Andreas Hochwagen,[5] G. Shirleen Roeder,[2,3,6] and Jennifer C. Fung[1,*]
[1]Department of Biochemistry and Biophysics, University of California, San Francisco, San Francisco, CA 94158, USA
[2]Howard Hughes Medical Institute
[3]Department of Molecular, Cellular, and Developmental Biology
Yale University, New Haven, CT 06520, USA
[4]Ingenuity Systems, Inc., Redwood City, CA 94063, USA
[5]Whitehead Institute for Biomedical Research, Cambridge, MA 02142, USA
[6]Department of Genetics, Yale University, New Haven, CT 06520, USA
[7]Present address: Marie Curie Research Institute, DNA Recombination Group, Oxted, Surrey RH8 0TL, UK
*Correspondence: jfung@biochem.ucsf.edu
DOI 10.1016/j.devcel.2008.07.006

SUMMARY

Tight control of the number and distribution of crossovers is of great importance for meiosis. Crossovers establish chiasmata, which are physical connections between homologous chromosomes that provide the tension necessary to align chromosomes on the meiotic spindle. Understanding the mechanisms underlying crossover control has been hampered by the difficulty in determining crossover distributions. Here, we present a microarray-based method to analyze multiple aspects of crossover control simultaneously and rapidly, at high resolution, genome-wide, and on a cell-by-cell basis. Using this approach, we show that loss of interference in *zip2* and *zip4/spo22* mutants is accompanied by a reduction in crossover homeostasis, thus connecting these two levels of crossover control. We also provide evidence to suggest that repression of crossing over at telomeres and centromeres arises from different mechanisms. Lastly, we uncover a surprising role for the synaptonemal complex component Zip1 in repressing crossing over at the centromere.

INTRODUCTION

As part of sexual reproduction, diploid parents undergo meiosis to produce gametes with a haploid complement of chromosomes (Roeder, 1997; Zickler and Kleckner, 1999). Central to this process is the segregation of homologous chromosomes at the first meiotic division. During prophase I, a high level of recombination is induced through the formation of double-strand breaks (DSBs) via the Spo11 protein (Keeney et al., 1997). A significant fraction (approximately half in budding yeast) of DSB repair events is accompanied by crossing over. Crossovers (COs) establish chiasmata, which are physical connections between homologs that promote proper chromosome segregation by correctly aligning chromosomes on the meiosis I spindle. Failure to sustain a CO on each pair of chromosomes can result in the production of aneuploid gametes; in humans, this leads to infertility, miscarriage, and developmental disabilities (Hassold et al., 2007).

To ensure that each chromosome pair receives at least one CO, crossing over is highly regulated. In most organisms, the spatial distribution of COs is tightly controlled through a process known as CO interference (Hillers, 2004; Jones, 1984; Muller, 1916). Interference ensures that COs are distributed nonrandomly along chromosome pairs to attain a more regular spacing between COs than would be expected for a random distribution. As a result, COs seldom occur close together.

Another manifestation of CO control is CO homeostasis, first described by Martini et al. (2006) as the means whereby normal levels of COs are maintained despite lowering the overall number of DSB-initiating events. CO homeostasis presumably reduces the chances of nondisjunction by ensuring that sufficient numbers of COs are made. Still unknown is how CO homeostasis is achieved or what its relationship is to interference since no mutants have been described that affect this process.

In spite of the importance of CO control, its molecular mechanisms remain elusive due, in large part, to the lack of an efficient and accurate way of measuring CO distribution. A typical method for measuring interference in budding yeast requires the manual dissection of tetrads containing the four progeny of a single meiosis. Only those tetrads that produce four viable spores are then scored for a limited number of genetic markers. Each tetrad is classified as having the parental ditype, tetratype, or nonparental ditype (NPD) arrangement of markers for each interval. To calculate interference, an NPD ratio is determined, which is the number of NPDs observed (approximately equivalent to double COs) divided by the number of NPDs expected based on the frequency of tetratypes (approximately equivalent to single COs) if COs were distributed randomly (Papazian, 1952). Accurate measurement of the NPD ratio requires dissection of large numbers of four-spore viable tetrads (typically hundreds to thousands), making the assessment of interference relatively difficult (Ott, 1991). Furthermore, meiotic mutants with defects in crossing over typically show poor spore viability, drastically reducing the number of four-spore viable tetrads that can

be obtained. As a result, mutants that might affect interference (e.g., mutants in recombination, chromosome structure, and synaptonemal complex assembly) are not routinely analyzed for interference defects.

An alternative method for measuring COs, which can be applied in analyzing interference, is direct allelic variation scanning of the genome (Winzeler et al., 1998). This method uses the nucleotide sequence variation between two yeast strains to evaluate the parental origins of progeny DNA resulting from a cross between them. By hybridizing total genomic DNA from the two different strains of yeast to high-density oligonucleotide arrays, Winzeler and coworkers identified a total of 3714 markers capable of distinguishing between the two strains. The inheritance pattern of these markers in the progeny strains was used to locate COs. The distribution of distances between adjacent COs can be used to measure interference. The advantage of this method is that very few four-spore viable tetrads would be needed to analyze interference, since interference would be assessed from all COs genome-wide, rather than from a few marked intervals.

Of the few mutants that have been examined genetically for loss of interference, at least two affect proteins that are components of the synapsis initiation complex (SIC), namely Msh4 and Zip4/Spo22 (hereafter referred to as Zip4) (Novak et al., 2001; Tsubouchi et al., 2006). SICs promote chromosome synapsis by facilitating polymerization of Zip1, a major building block of the synaptonemal complex (Sym et al., 1993). Zip2, Zip3, Zip4, Msh4, and Msh5 (a.k.a., ZMM proteins; Lynn et al., 2007) are all components of the SIC. Mutations affecting all known SIC components reduce crossing over, and SICs display interference (Fung et al., 2004), suggesting that SICs are the same as, or associated with, a large CO-promoting complex assembly known as the late recombination nodule (Carpenter, 1988).

Until recently, a reasonable assumption would have been that all SIC mutants show the same level of interference since all show a similar reduction in crossing over. However, a recent study of the *zip4* mutant (Tsubouchi et al., 2006) reported evidence for negative interference, which differs from the absence of interference found for *msh4* (Novak et al., 2001; Sym and Roeder, 1994). Negative interference implies a different kind of nonrandom distribution, where COs are clustered together, instead of being spaced far apart. However, apparent negative interference can arise from variations in CO frequencies within a population of cells showing no interference (Sall and Bengtsson, 1989), an aspect that is difficult to assess genetically. Adding to the confusion, a more recent study of interference in several ZMM mutants reports normal interference for *zip4* (Shinohara et al., 2008). A key benefit of the microarray analysis is its ability to address whether variations in recombination exist within a population, since the analysis is performed on a cell-by-cell basis, unlike genetic measurements that are inherently population based; thus, apparent versus true negative interference can be distinguished.

Besides interference and homeostasis, many organisms have additional mechanisms to modify the CO landscape that can potentially influence CO control. Both recombination hotspots (Petes, 2001) and the suppression of COs near telomeres (Su et al., 2000) and centromeres (Lambie and Roeder, 1986) are known to contribute to the nonuniformity of CO distribution. Crossing over near centromeres and/or too far from them can be detrimental to chromosome segregation and increases the risk of producing aneuploid progeny (Koehler et al., 1996a; Lacefield and Murray, 2007; Lamb et al., 1996; Rockmill et al., 2006). Analysis of COs in the vicinity of telomeres and centromeres could be greatly aided by a genome-wide approach in which crossing over near these chromosomal landmarks can be easily assessed.

In this paper, we show that mapping COs by DNA microarrays is a powerful approach for assessing CO control. We show that all metrics of crossing over previously determined genetically can be recapitulated with this genomic approach. Gene conversions (GCs) can also be assessed, but in a more limited fashion than COs. For the first time (to our knowledge), we identify mutants, *zip2* and *zip4*, that show a reduction in CO homeostasis. Our analyses of COs and GCs not associated with COs (NCOs) at telomeres and centromeres suggest that different mechanisms are responsible for CO repression at these sites. At telomeric ends, COs are repressed due to a change in the relative proportions of COs versus NCOs, while COs near centromeres are reduced most likely by favoring repair between sister chromatids versus interhomolog repair. Finally, we show that this centromeric repression is dependent on Zip1.

RESULTS

Genome-Wide Analysis of Recombination Using DNA Microarrays

The tetrads genotyped in this study resulted from a cross between a standard laboratory strain, S96 (an S288c derivative), and a clinical isolate, YJM789 (Wei et al., 2007). The sequence difference between these strains (0.6%) is high enough to achieve the resolution required to detect COs, but not so high as to act as a barrier to recombination (Figure S1 and Supplemental Results, available online). Spore viability and sporulation frequency are provided in Table S1 for strains derived from these parents. Sequence differences between the two parental strains were used to determine the parental origin of progeny DNA in each tetrad.

In this study, about 8000 markers (probe sequences), whose hybridizations show differential signals between the two parental strains, were scored. The mean distance between markers is 1.5 kb (~0.5 cM); overall, markers are uniformly distributed across the genome with only a few noticeable gaps (Figure 1A). The distribution of intermarker distances is shown in Figure 1B. Because four-spore viable tetrads are examined, markers showing reciprocal exchange can be unambiguously identified as COs; markers showing 3:1 and 1:3 configurations are identified as GCs, whereas 4:0 and 0:4 configurations often indicate premeiotic recombination events.

Microarray data from 26 wild-type tetrads show that, on average, 98.0% of the markers segregate 2:2; 2.0% of the markers segregate 1:3 or 3:1; and less than 0.1% of the markers segregate 4:0 or 0:4 (Table S2), in good agreement with genetic data that reports 95% of markers segregating 2:2 and 4.8% showing non-2:2 segregations (Fogel et al., 1978).

Good Agreement Found for CO Frequency and Density

Examination of CO frequency reveals a mean of 95 (±10 standard deviation [SD]) COs per meiosis (Figure 1C and Table 1), on par

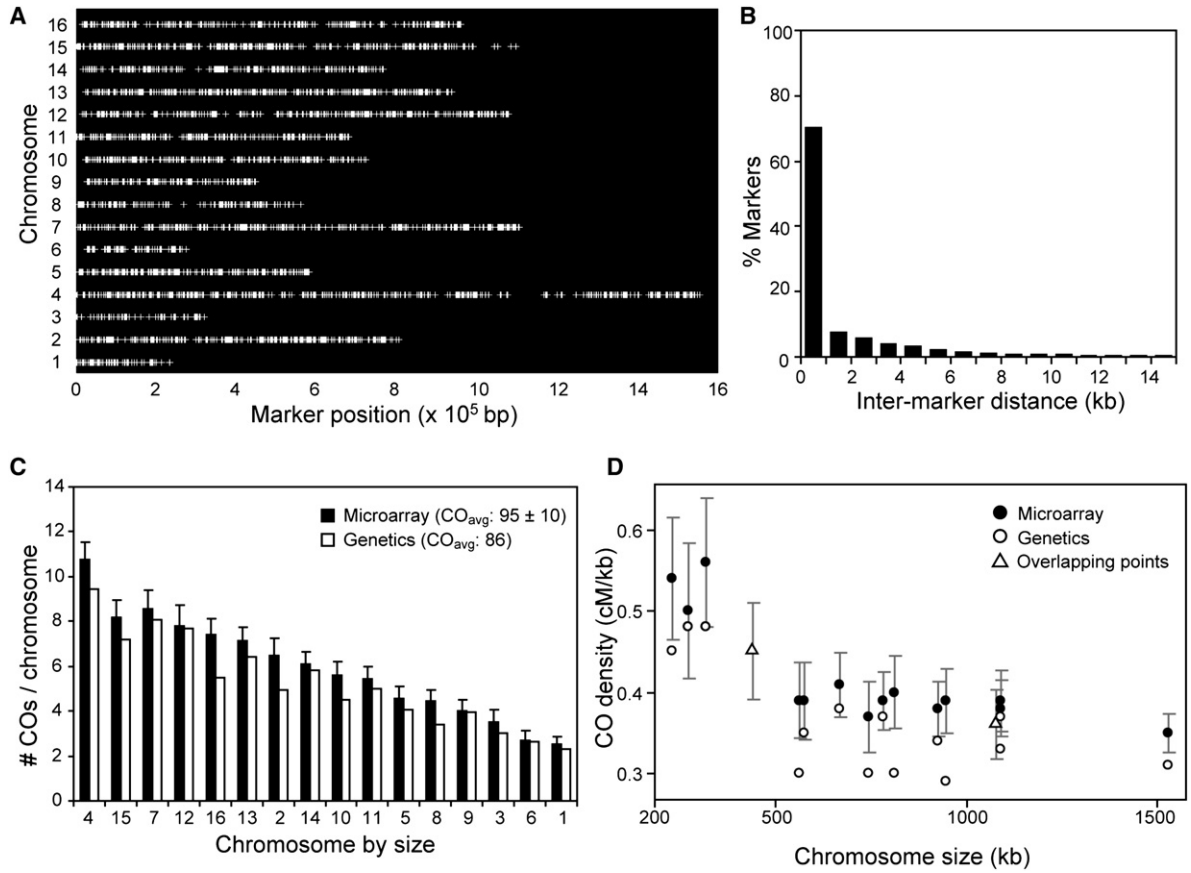

Figure 1. Characterization of Crossover Distribution in Wild-Type

(A) Marker distribution for all 16 chromosomes in the S96/YJM789 strain. Vertical bars indicate the location of markers.

(B) Plot of frequency of intermarker distances. Over 78% of the markers are spaced less than 2 kb apart. Mean distance is 1.5 kb.

(C) Mean number of COs per chromosome and total COs per meiosis were compared between microarray data and genetic map data obtained from the *Saccharomyces* Genome Database (SGD). Error bars denote 95% confidence interval (C.I.) of the microarray data.

(D) Comparison of CO density between microarray and genetic data; 95% C.I.s are shown for microarray data.

with the 86 COs per meiosis computed from map distances compiled from several genetic studies (Cherry et al., 1997) (*Saccharomyces* Genome Database [SGD], http://www.yeastgenome.org/). The slightly greater value for COs seen here may be due to a better overall marker resolution compared to the marker resolution of the genetic map. Alternatively, the slight increase in map distance might reflect increased numbers of events due to repeated cycles of heteroduplex rejection characteristic of polymorphic strains (Borts and Haber, 1987). Figure 1C shows good agreement of CO frequency on a per-chromosome basis. A plot of CO density against chromosome size reveals that smaller chromosomes have a higher density of COs than larger chromosomes (Figure 1D), a trend consistent with previous genetic observations (Kaback et al., 1992).

No Chromatid Interference

Unlike standard genetic analysis using phenotypic markers, the microarray approach allows a straightforward analysis of chromatid interference (where a CO between any two nonsister chromatids affects the probability of those chromatids being involved in neighboring COs), since the chromatids involved in each CO are known. Previous studies report no chromatid interference in wild-type strains as assayed by the ratio of two-, three-, and four-strand double COs between adjacent COs (Perkins, 1962). In wild-type (Table 1), we see no difference from the 1:2:1 ratio expected for no chromatid interference ($\chi^2 = 1.46$, $p = 0.5$), consistent with previous genetic studies.

Repression of COs near Telomeres and Centromeres

Telomere- and centromere-proximal regions have reduced CO frequency relative to the rest of the chromosome (Lambie and Roeder, 1986, 1988; Su et al., 2000). To determine whether our microarray data detects a reduction in COs in these regions, we examined the distribution of telomere-CO and centromere-CO distances. The distance between every CO and the nearest chromosome end (determined from SGD) was obtained and the resulting histogram is shown in Figure 2A. We observe a 7-fold repression within 20 kb of the chromosome end, as compared with regions farther away from the telomeres. Elevated CO levels as compared with what was expected for a simulated distribution were seen 20–140 kb away from the chromosome end (Figure 2A), in agreement with a recent study of crossing over at

Table 1. Summary of Crossover Data

	Recombination		Crossover Count				Chromatid Interference				
Strains	Array	Genetics	# of Tetrads	Total	Mean	SD	2 s.d.	3 s.d.	4 s.d.	Ratio	p value
WT	1.0	1.0	26	2474	95.2	10.2	538	1010	510	1.0: 1.9: 1.0	0.48
zip1	1.2	0.4–0.8[a]	9	987	109.7	18.1	245	416	187	1.0: 1.7: 0.8	0.05
zip2	0.5	0.5–0.8[b]	26	1272	49.0	9.3	232	442	218	1.0: 1.9: 0.9	0.77
zip3	0.6	0.3–0.8[c]	8	416	52.0	8.3	78	142	76	1.0: 1.8: 1.0	0.77
zip4	0.6	0.3–0.9[d]	34	1927	56.7	17.0	341	667	362	1.0: 2.0: 1.0	0.45
msh4	0.4	0.4–0.6[e]	11	405	36.8	8.7	66	113	60	1.0: 1.7: 0.9	0.60
spo16	0.6	0.5	8	422	52.8	12.4	96	131	72	1.0: 1.4: 0.8	0.07
ndj1	1.0	0.9– 1.4[f,g]	7	695	99.3	19.0	174	267	149	1.0: 1.5: 0.9	0.03
sgs1	1.1	1.3[h]	11	1163	105.7	14.0	266	476	248	1.0: 1.8: 0.9	0.34

For chromatid interference, ratios were normalized to the two-strand double (s.d.) CO. Chi-square analysis for wild-type and all mutants showed no difference from the expected 1:2:1 ratio if there was no chromatid interference (p = 0.01).
[a] Sym and Roeder (1994).
[b] Chua and Roeder (1998).
[c] Agarwal and Roeder (2000).
[d] Tsubouchi et al. (2006).
[e] Novak et al. (2001).
[f] Chua and Roeder (1997).
[g] Wu and Burgess (2006).
[h] Rockmill et al. (2003).

chromosome ends (Barton et al., 2008). To determine whether this elevation of CO frequency is due to the inclusion of small chromosomes that have a higher CO density than other chromosomes, we reanalyzed the telomere-CO distances excluding the four smallest chromosomes (Figure 2B). Removal of the smallest chromosomes eliminated most of the observed elevation in CO frequency; however, some elevation of CO frequency remained, though at defined intervals 40–60 kb and 140–160 kb away from the ends.

Recent analyses of genome-wide DSB hotspot distributions (Blitzblau et al., 2007; Buhler et al., 2007) reported an ~2-fold repression of DSBs within 20 kb of the chromosome end. Such a repression of DSBs could contribute to the observed lower level of crossing over. However, when telomere-NCO distances were examined, no concomitant repression of NCOs was seen in the 20 kb region nearest the chromosome end; instead, the NCO level was within the range predicted by the simulation and in accordance with the level found in neighboring intervals (Figures 2C and 2D). The fact that DSB levels are repressed, but NCO levels remain unchanged, suggests that the repression of COs reflects a change in the CO:NCO ratio (in favor of NCOs) rather than an alteration in overall levels of DSBs or a switch from interhomolog to intersister repair.

Centromeric repression of meiotic recombination has been well documented in budding yeast (Lambie and Roeder, 1986) and other higher eukaryotes (Hassold et al., 1996; Koehler et al., 1996b). To test whether CO repression at the centromere can be seen in the wild-type distribution of COs, we measured the centromere-CO distance for every CO. Figures 2E and 2F show that crossing over within 10 kb from the centromere is decreased 6-fold, compared with neighboring intervals greater than 10 kb away. Unlike those of the telomere, measurements of centromere-NCO distances do show a repression of NCO frequency (6-fold) at the most proximal interval to the centromere (Figures 2G and 2H). Therefore, CO repression at the centromere is less likely to occur via modification of the CO:NCO ratio as it is at telomeres, but is more likely to result from mechanisms that either alter the number of DSBs or change the bias from interhomolog to intersister repair. Thus, the mechanisms by which CO repression is attained at the centromere and the telomere appear to be different.

Determination of CO Interference with Only a Few Tetrads

The aforementioned results show that the microarray-based analysis can recapitulate previous measurements of CO frequency. But can microarray-based measurements recapitulate numerical estimates of interference in wild-type? Inspection of the microarray results shows that wild-type COs are relatively evenly spaced and no chromosome is without at least one CO (Figure 3A), indicating that CO distribution is regulated in a manner qualitatively consistent with the existence of interference (compare with Figure 3B showing a loss of interference). Quantitative comparison is more difficult because the NPD ratio, which is a well-known metric for interference, is an inherently population-based measure, requiring large numbers of tetrads for reliable statistics. Because our measurements are based on analyzing a small number of tetrads, we could not directly calculate the NPD ratio for any given marker pair with statistical accuracy. Instead, to determine whether the level of interference obtained by microarrays is quantitatively similar to that obtained genetically via NPD ratios, we employed a method in which interference measured by inter-CO distances is converted into an NPD ratio using Monte Carlo simulation.

Briefly, inter-CO distances were measured and fitted with a gamma distribution function characterized by a shape (γ) and scale (β) parameter. The gamma distribution arises in statistical studies of the distributions of intervals between successive

random events; hence, it is a natural choice for a distribution to describe the intervals between successive COs. The gamma distribution is a useful tool for estimating interference levels since γ itself can be used as a measure of the strength of interference. A value of $\gamma = 1$ corresponds to no interference, whereas $\gamma > 1$ indicates positive interference with larger values of gamma indicating stronger interference (McPeek and Speed, 1995; Zhao et al., 1995). Experimentally obtained inter-CO distances are well fit by the gamma distribution for wild-type (Figure 4A; $\chi^2 = 4.2$, $p > 0.99$, Figure S2A [smaller bin size]) and for *zip4* (Figure 4B; $\chi^2 = 12.7$, $p = 0.63$, Figure S2B).

The parameters of the gamma function do not directly tell us the value expected for the NPD ratio; hence, we used a simulation-based approach to estimate the NPD ratio from the gamma distribution. From the best-fit parameters of the gamma distribution, a conditional probability function (hazard function) was determined that gives the probability of a CO arising at a particular distance from a pre-existing CO (Figure 4C; details on the gamma distribution are given in the Supplemental Procedures). This function was then used as the basis for simulating CO positions for a large population of tetrads to back-calculate a simulated value for the NPD ratio (see Supplemental Procedures for details on the simulation of NPD ratios). Applying this analysis to wild-type inter-CO distances, a best-fit gamma value of 1.94 was found; this in turn gave a simulated NPD ratio value of 0.38, which is in good correspondence with the mean NPD ratio of 0.32 obtained from published values of wild-type interference for intervals with a mean size of 30 cM. The gamma value of 1.94 concurs with a previously reported gamma value ($\gamma = \sim 2$) for *Saccharomyces cerevisiae* (Foss and Stahl, 1995), confirming that interference in budding yeast is not as strong as in other organisms, such as *Drosophila* ($\gamma = \sim 4$) (calculated in Foss and Stahl, 1995), *Arabidopsis thaliana* ($\gamma = \sim 3$) (Copenhaver et al., 2002), or *Mus musculus* ($\gamma = \sim 10$) (Broman et al., 2002; de Boer et al., 2006). Although this analysis encompassed data from all 26 wild-type tetrads, we find that even 3 tetrads provide a sufficient number of inter-CO distances (~250) to assess interference levels (data not shown). Figure S3 shows interference calculated from our microarray data by an adaptation of the method devised by Malkova et al. (2004) to measure the extent of interference on adjacent intervals. The maximum effective distance over which interference extends is ~150 kb, in agreement with the 154.2 kb reported in the Malkova study (Figure S3A). The effective distance over which interference acts can also be obtained directly from the hazard function (Figure 4C).

One final aspect of interference that could be tested is whether NCOs show a lack of interference. Studies in fungi report that NCOs, unlike COs, do not exhibit interference (Malkova et al., 2004; Mortimer and Fogel, 1974). To see if a similar effect is seen with NCOs observed in DNA microarrays, we first eliminated any GCs associated with the formation of a CO (GC_{CO}s) before calculating distances between the remaining NCOs. Because there were on mean only 50 detectable GCs per tetrad (31 GC_{CO}s, 19 NCOs; Tables 1 and 2), many more wild-type tetrads were needed (~26) to accumulate enough inter-NCO distances to measure interference. The NCOs observed do not exhibit interference ($\gamma = 1.1$, corresponding to a predicted NPD $ratio_{sim} = 0.9$). By this analysis, NCOs observed by microarrays behave as expected based on tetrad analysis.

CO Homeostasis Measured from Microarray Data

CO homeostasis assures that CO numbers are maintained within a narrow range of fluctuation despite fluctuations in the number of DSBs from cell to cell. Analysis of the correlation between COs and NCOs provides a test for CO homeostasis by reporting the level of correlation between NCOs and COs in individual tetrads, over the ensemble of tetrads. The correlation coefficient is not a measure of quantitative change of one variable with respect to another, but it is a measure of intensity of association between two variables (see the Experimental Procedures for more details). For ideal homeostasis, the number of COs would be independent of the number of NCOs, giving a correlation coefficient of zero. No homeostasis would result in a correlation coefficient of one. The wild-type correlation coefficient is −0.07, indicating nearly ideal homeostasis, in agreement with an earlier observation for CO homeostasis (Martini et al., 2006).

Marker Resolution Influences GC Detection

Markers showing 3:1 or 1:3 configurations indicate a GC event. In general, contiguous markers having the same pattern of 3:1 or 1:3 chromatid arrangements are considered to be part of a single GC event. The mean number of events and mean tract length for both GC_{CO}s and NCOs are provided in Table 2; however, caution is warranted before making comparisons with the GC data, so that detection issues are taken into account.

Although there is excellent detection of COs, GC detection is limited by our current marker density. If the mean GC tract length is 1.5 kb (Borts and Haber, 1987), but the mean distance between markers is only 1.5 kb (Figure 1B), our study will underestimate the actual frequency of GCs because some strand exchange events will fail to include a scorable marker. The GC comparisons presented here in this study either take into account the detection issue or are not unduly affected by the detection limitation.

To estimate the proportion of GCs detected out of all GCs, we divided the mean number of NCOs (18.6) by an estimate of the total expected number of NCOs (66.1) based on a higher resolution tiling array analysis of the same wild-type strain (Mancera et al., 2008). This calculation results in a detection level of 28% of the actual number of GC events compared with the 70% detection of NCOs by Mancera et al. (2008). Since detection is not equal for GCs with small versus long GC tract lengths, the subpopulation we do detect will be biased toward GCs with longer tract lengths (Figure S4). One implication of this unequal detection of GC tracts is that any comparison made where there is a potential difference in GC tract lengths between the two populations must factor in how the change in detection might affect the comparison.

Conversion tract lengths differ between COs and NCOs (Baudat and de Massy, 2007). The medians of GC_{CO} and NCO tract lengths of wild-type were compared (Table 2 and Table S3). GC_{CO} tract lengths (4.4 kb) were found to be significantly larger than NCO tract lengths (3.9 kb), in agreement with observations in mice and humans (Guillon et al., 2005; Jeffreys and May, 2004).

CO Levels in Mutants Agree with Genetic Data, Except for *zip1*

To test the usefulness of the microarray analysis in measuring CO control in mutants, we looked at eight mutants with known or

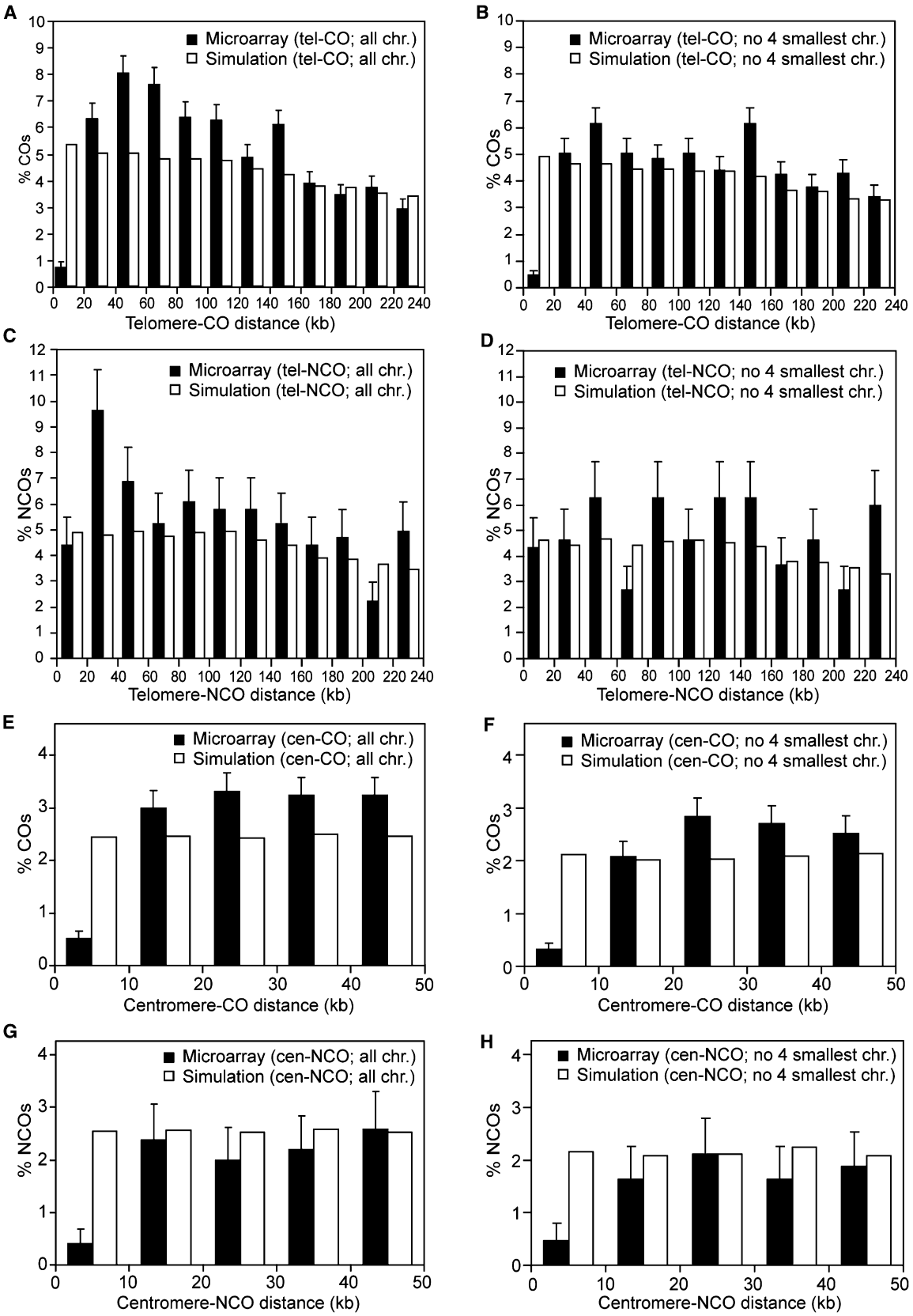
A
Microarray (tel-CO; all chr.)
Simulation (tel-CO; all chr.)
% COs
Telomere-CO distance (kb)
B
Microarray (tel-CO; no 4 smallest chr.)
Simulation (tel-CO; no 4 smallest chr.)
% COs
Telomere-CO distance (kb)
C
Microarray (tel-NCO; all chr.)
Simulation (tel-NCO; all chr.)
% NCOs
Telomere-NCO distance (kb)
D
Microarray (tel-NCO; no 4 smallest chr.)
Simulation (tel-NCO; no 4 smallest chr.)
% NCOs
Telomere-NCO distance (kb)
E
Microarray (cen-CO; all chr.)
Simulation (cen-CO; all chr.)
% COs
Centromere-CO distance (kb)
F
Microarray (cen-CO; no 4 smallest chr.)
Simulation (cen-CO; no 4 smallest chr.)
% COs
Centromere-CO distance (kb)
G
Microarray (cen-NCO; all chr.)
Simulation (cen-NCO; all chr.)
% NCOs
Centromere-NCO distance (kb)
H
Microarray (cen-NCO; no 4 smallest chr.)
Simulation (cen-NCO; no 4 smallest chr.)
% NCOs
Centromere-NCO distance (kb)

potential interference defects. The *zip1*, *zip4*, *msh4*, *ndj1*, and *sgs1* mutants have been previously shown to be defective in interference, albeit to different extents (Chua and Roeder, 1997; Novak et al., 2001; Rockmill et al., 2003; Sym and Roeder, 1994; Tsubouchi et al., 2006; Figure 5A. We also included *zip2* and *zip3*, whose gene products are part of the SIC (Agarwal and Roeder, 2000; Chua and Roeder, 1998), but whose levels of interference were unknown at the initiation of this study. In addition, we analyzed a mutation in the *SPO16* gene, which has recently been shown to encode a SIC component; the *spo16* mutant has been reported to show normal levels of CO interference (Shinohara et al., 2008).

In general, the change in CO levels for the mutants as determined by microarray agrees with values reported in prior genetic studies (Table 1) and with the genetic data obtained in this study (Table S4). The only notable exception is *zip1*. Instead of the 2-fold decrease in COs found for *zip1* in genetic and physical studies (Storlazzi et al., 1996; Sym et al., 1993), *zip1* shows an increase in COs (110 COs/tetrad) over those of wild-type (95 COs/tetrad; Table 1). Our hypothesis is that in the case of *zip1*, only a selected population of cells (a subset with high levels of crossing over) produces tetrads in the S96/YJM789 diploid. Indeed, the frequency of asci containing four spores is orders of magnitude lower in *zip1* than in the mutants affecting SIC proteins (Table S1), suggesting that the *zip1* mutant has additional difficulties not experienced by the SIC mutants. Consistent with the notion that we are looking at a selected subset of meioses in *zip1*, we find a 2-fold increase in NCOs in *zip1* as compared with other ZMM mutants (i.e., *zip2* and *zip4*).

Changes in GC Tract Lengths

All mutants, except *msh4* and *ndj1*, show increased NCO frequencies (Table 2 and Table S5). Because an increase in NCO tract length could give rise to an apparent increase in NCO frequency, NCO tracts lengths were examined using a nonparametric multicomparison median test (Levy, 1979) to determine if NCO tract lengths are significantly different between the different strains (Table S6). Only for wild-type, *zip1*, *zip2*, *zip4*, and *sgs1* were sample sizes large enough to perform this test. The results show that the NCO tract lengths of *zip1*, *zip2*, and *zip4* are significantly greater than those of wild-type (Table S6). Whether the ~2-fold difference seen in NCO frequencies in *zip2* and *zip4* over wild-type can be entirely attributed to the increase in tract length remains to be seen. However, it is doubtful that an increase in tract length is responsible for the additional 2-fold increase (above *zip2* and *zip4*) in NCO frequency seen for *zip1*, since no significant differences were seen among tract lengths for *zip1*, *zip2*, and *zip4*. The same conclusions can be drawn for GC_{CO} tract lengths (Table S6). Because the median NCO tract length in *sgs1* does not differ from that of wild-type, the increase in NCO frequency in *sgs1* is likely a true increase in the number of NCOs and not an artifact of detection.

Analysis of CO Interference, Chromatid Interference, and E_0s in Mutants

A representative example of CO distributions for a mutant (*zip4*) with reduced interference is shown in Figure 3B. In *zip4*, where loss of interference is expected (Tsubouchi et al., 2006), COs are less evenly spaced, despite the overall reduced number of COs. Figure 5A plots the array-derived interference values against the mean genetic values for all mutants. For comparison, published measurements of interference assayed genetically were used, except for *zip2*, *zip3*, and *spo16*, for which tetrads were dissected (Table S4). In most cases, microarray-based interference levels for the mutants agree well with the genetic data (Figure 5A). The two exceptions are *zip4* and *ndj1*. The *zip4* mutant shows a loss of interference, not normal interference or negative interference, both of which have been reported in different studies (Shinohara et al., 2008; Tsubouchi et al., 2006). In *ndj1*, wild-type interference is found, instead of a moderate decrease in interference (Chua and Roeder, 1997). The *spo16* mutant shows a decrease in interference similar to that shown by the other SIC mutants (Figure 5A). Examination of chromatid interference in the mutants showed no significant difference in the 1:2:1 ratio expected for no chromatid interference (Table 1). Lastly, all mutants show increased numbers of E_0s, defined as chromosome pairs that lack any COs (Table S7). Because only four-spore viable tetrads were examined in our microarray analysis, the number of E_0s represents a minimal estimate of the E_0 frequency. E_0s are seen more frequently for smaller chromosomes, although E_0s for larger chromosomes are observed as well. In the majority of tetrads, zero or one E_0 was the norm, although four E_0s were observed in one *msh4* tetrad (data not shown).

Negative Interference in *zip4* Mutant May Arise from Variations in CO Frequency

The *zip4* mutant has been reported to display negative interference, a phenomenon that can be explained either by the tendency of COs to cluster or by variation in CO frequency within a cell population having no interference (see the INTRODUCTION). The latter effect can arise because measurements of NPD ratios require the assumption of a known and constant CO frequency. It is impossible to assess the cell-to-cell variations in CO frequency using population-based genetic techniques. However, the microarray approach enables analysis of individual meioses and thus is uniquely powerful in addressing such questions.

To assess whether *zip4* has true or apparent negative interference, CO number was examined on a tetrad-by-tetrad basis to look for outliers as evidence for the existence of a separate population of *zip4* tetrads with a higher CO frequency. Figure 5B shows the distribution of CO numbers per meiosis for wild-type, *zip4*, and *zip2* for which larger numbers of tetrads were available. An outlier is observed only for *zip4*, and not for wild-type or *zip2*. Table S8 shows how the inclusion of the outlier results in less interference than when the outlier has been excluded. Although apparent

Figure 2. CO and NCO Distributions near Telomeres and Centromeres in Wild-Type

Distribution of COs and NCOs relative to the nearest telomere (A–D) or centromere (E–H). Microarray data from wild-type is plotted against a simulated distribution that incorporates interference but assumes a uniform CO landscape along the chromosome. (B), (D), (F), and (H) show distributions without the four smallest chromosomes (I, III, VI, and IX). Error bars = SD.

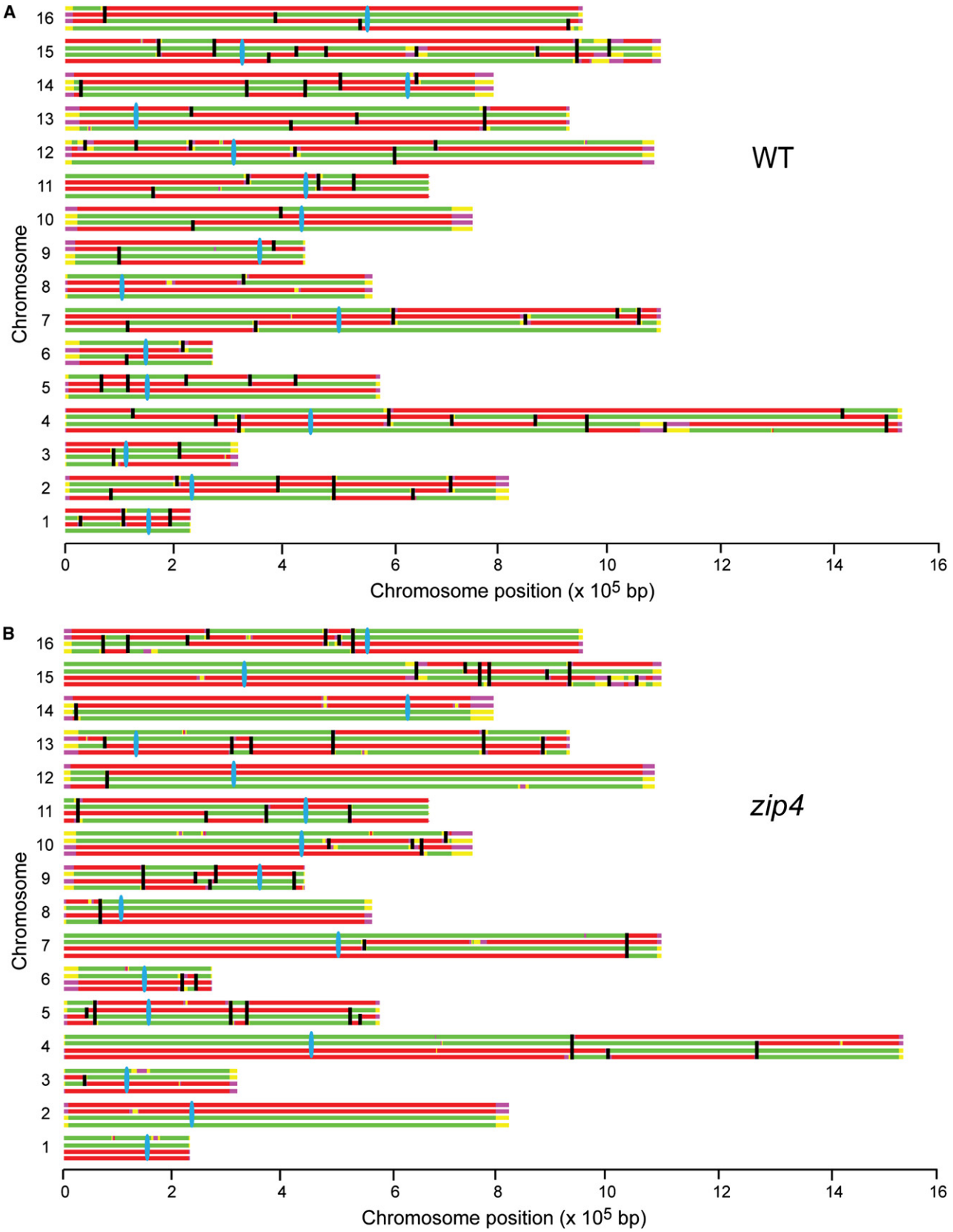
A
WT
Chromosome
16
15
14
13
12
11
10
9
8
7
6
5
4
3
2
1
0
2
4
6
8
10
12
14
16
Chromosome position (x 10^5 bp)
B
zip4
Chromosome
Chromosome position (x 10^5 bp)

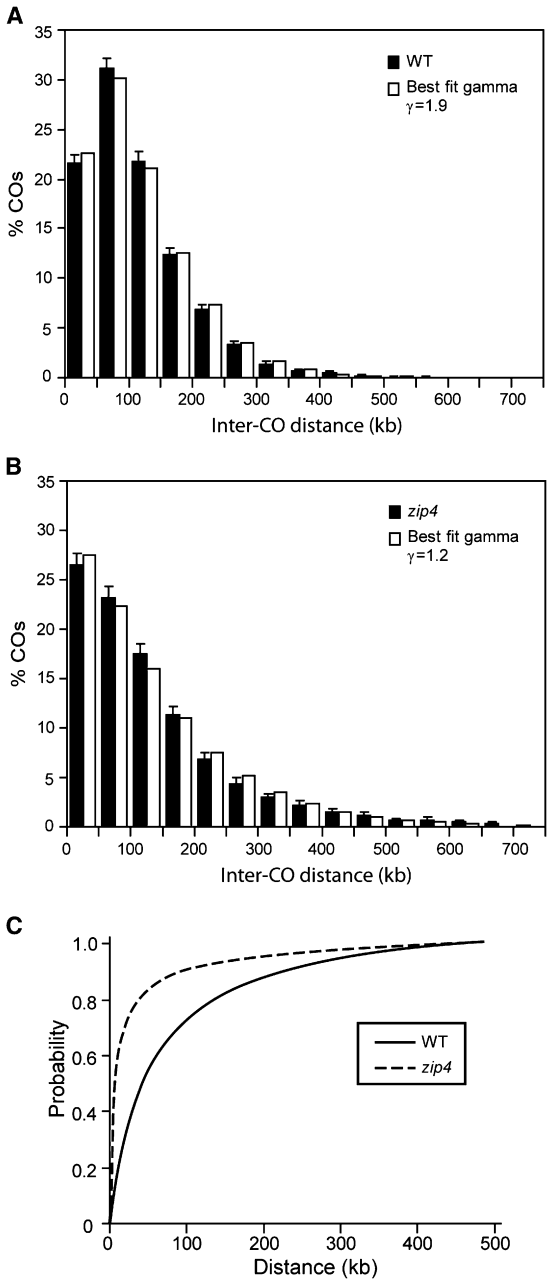

Figure 4. Determination of Interference

Comparison of the experimental and best-fit gamma distribution for inter-CO distances for wild-type with normal interference (A) and *zip4* with reduced interference (B). $\gamma = 1$ indicates no interference, while $\gamma > 1$ indicates positive interference. (C) Hazard functions are calculated from the best-fit gamma distribution parameters for wild-type (WT) (solid line) and *zip4* (dotted line). Errors bars = SD.

negative interference arises when there is a variation in the recombination frequency within a population having no interference, the effect is the greatest when only a small fraction of the population (<10%) has much larger recombination levels relative to the rest of the population (Figure 1 in Sall and Bengtsson, 1989). This is exactly what is seen in *zip4*, where 1 out of 34 tetrads exhibits a higher level of crossing over than the remainder of the population (Figure 5B). Taken together with the facts that regional clustering is not apparent in the CO spatial distribution (data not shown) and that a loss of interference is observed by our approach, these considerations suggest that the negative interference observed genetically may result from the existence of more than one population of tetrads, rather than actual clustering of COs.

CO Homeostasis Is Perturbed in *zip2* and *zip4*

CO homeostasis analysis was confined to mutants with a sufficient number of tetrads, namely *zip2* and *zip4*. Any change in CO homeostasis would be reflected as an increase or decrease in the correlation coefficient. For both *zip2* and *zip4*, a decrease in CO homeostasis is indicated by significant increases in correlation coefficients (0.44 and 0.34, respectively), as compared with −0.07 in the wild-type control (Figure 5C).

Centromeric Repression of Recombination Is Relieved in a *zip1* Mutant

Do any of the mutants relieve the telomeric or centromeric repression of COs? Of the eight mutants examined, only the *zip1* mutant has any effect at the centromere. Crossing over in *zip1* is no longer repressed in the 10 kb region closest to the centromere and is comparable to the levels of crossing over more distal to the centromere (Figure 6A). No relief of telomeric repression is seen in any of the mutants tested (data not shown).

Does Zip1 affect crossing over per se or does it prevent DSBs from occurring near centromeres? To answer this question, we compared the frequency of NCOs proximal to the centromere in wild-type and *zip1*. In contrast to wild-type (Figures 2G and 2H), the frequency of NCOs for *zip1* within 10 kb nearest the centromere is equal to the frequencies found in noncentromeric regions (Figure 6B), thus paralleling the increase in COs seen in *zip1*. The CO:NCO ratio in this proximal interval is not significantly different between wild-type (1.31 ± 1.0 SD) and *zip1* (0.75 ± 0.18) and is thus unaffected by the *zip1* mutation.

Genetic Measurements Confirm that NCO Levels Change at Centromeres in *zip1*

Given that our *zip1* strain shows higher levels of crossing over than expected based on genetic and physical data, it is possible that the high level of COs at centromeres is true only for the subpopulation of *zip1* cells that exhibit the overall high levels of crossing over. To address this concern, we performed a genetic analysis of recombination near the centromere of chromosome III in a BR1919 strain. The haploid parents are identical throughout the genome, except for a small number of well-defined genetic

Figure 3. CO Distribution Pattern for Wild-Type and *zip4*

Shown are CO distributions from representative tetrads from wild-type (WT) (A) and *zip4* (B). Black vertical bars indicate the location of COs, and blue bars indicate centromeres. S96 parental origin is displayed in green; YJM789 parental origin is shown in red. Yellow (S96) and magenta (YJM789) indicate less confidence (<99% probability) in the designation of marker origin. Yellow and magenta sections at the ends of chromosomes are extrapolations from the last known marker nearest the end.

Table 2. Summary of Gene Conversion Data

	Gene Conversion Not Associated with CO (NCO)							Gene Conversion Associated with CO (GC_{CO})							
	Count		Tract length (kb)			Markers per NCO		Count		Tract length (kb)			Markers per GC_{CO}		
	Mean	SD	Mean	SD	Median	Mean	% NCO>1 Marker	Mean	SD	Mean	SD	Median	Mean	% GC_{CO}>1 Marker	Mean % GC_{CO}/CO
WT	18.6	8.7	5.1	32.5	3.9	3.3	79	30.7	5.1	5.9	5.2	4.4	3.1	65	32.5
zip1	71.3	17.4	6.3	5.2	5.1	3.9	79	61.4	9.5	7.9	7.9	6.3	4.1	73	57.3
zip2	30.3	10.1	5.8	4.4	4.7	4.1	78	26.0	6.8	7.6	7.7	5.8	4.2	72	53.0
zip3	37.0	8.9	5.9	5.3	4.6	4.1	83	29.0	4.1	7.4	6.4	5.8	3.9	70	57.1
zip4	35.1	14.8	6.3	5.4	5.0	3.8	78	28.3	11.0	7.3	6.5	5.7	4.0	71	51.0
msh4	17.2	6.5	5.5	5.1	4.2	2.9	68	17.0	6.5	6.5	3.9	5.8	3.6	72	45.9
spo16	33.9	8.5	6.6	5.1	5.3	3.7	82	28.1	7.9	7.9	5.9	6.4	3.5	70	54.3
ndj1	21.6	8.4	6.2	5.6	5.3	5.0	85	36.0	10.9	6.2	5.0	4.9	3.6	63	37.5
sgs1	36.4	25.4	6.4	8.8	4.1	4.2	87	39.5	10.0	6.0	5.2	4.8	3.7	70	36.3

The average number of markers involved in detecting each gene conversion is reported for NCO and GC_{CO}. Percentage of NCO and GC_{CO} detected by more than one marker is shown.

markers. In this strain background, the sporulation efficiency and spore viability of *zip1* is comparable to that of the SIC mutants.

To assay the level of recombination at the centromere, we used a strain carrying *URA3* heteroalleles adjacent to the centromere of chromosome III so that gene convertants (i.e., Ura^+ prototrophs) could be selected (Figure 6C). We found an 8-fold increase in Ura^+ recombinants in *zip1* relative to wild-type (Figure 6D), strongly supporting the idea that interhomolog

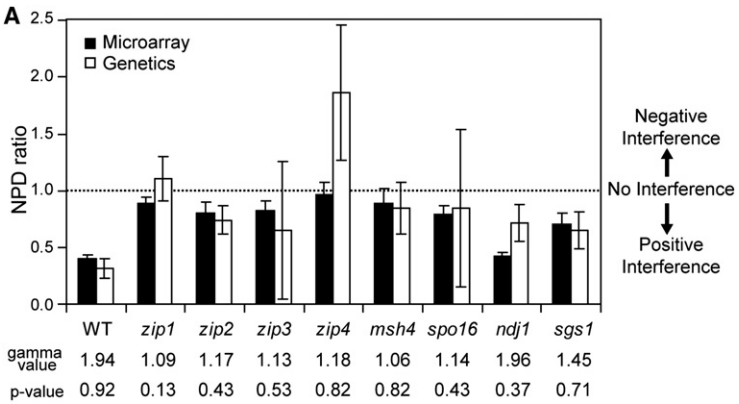

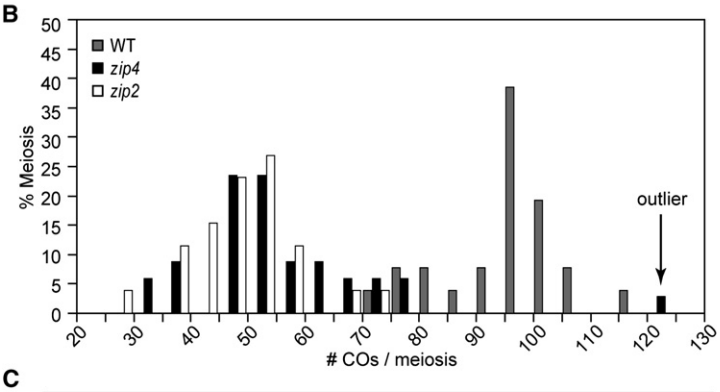

C

	Correlation Coefficient				
	WT	mutant	q	q'	Conclusion
WT vs. *zip4* (all data)	-0.07	0.34	2.09	1.64	Reject H_0
WT vs. *zip4* (no outlier)	-0.07	0.67	3.89	1.64	Reject H_0
WT vs. *zip2*	-0.07	0.44	2.44	1.64	Reject H_0

Figure 5. *zip4* and *zip2* Show Reduced CO Homeostasis

(A) Comparison of interference determined by microarray (simulated NPD ratio) and genetic approaches (NPD ratio). Genetic NPD ratios were obtained by averaging published NPD ratios; simulated NPD ratios were determined in this study (Table S4). Error bars = SD. Best-fit gamma values are shown. $p > 0.05$ shows that the best-fit inter-CO distribution fits well with the experimental distribution, as determined by chi-square analysis.

(B) Dispersion of CO number per meiosis for WT (n = 26; in gray), *zip4* (n = 34; in black), and *zip2* (n = 26; in white). Black vertical arrow indicates the outlier *zip4* tetrad with 126 COs.

(C) Comparison of a control correlation coefficient (wild-type) against mutants using an analog to the Dunnett's test (Huitema, 1974). Correlation coefficients were calculated based on the numbers of COs and NCOs. q' denotes critical value of $q_{0.05,\infty,3}$. $q > q'$ rejects the hypothesis that correlations are the same.

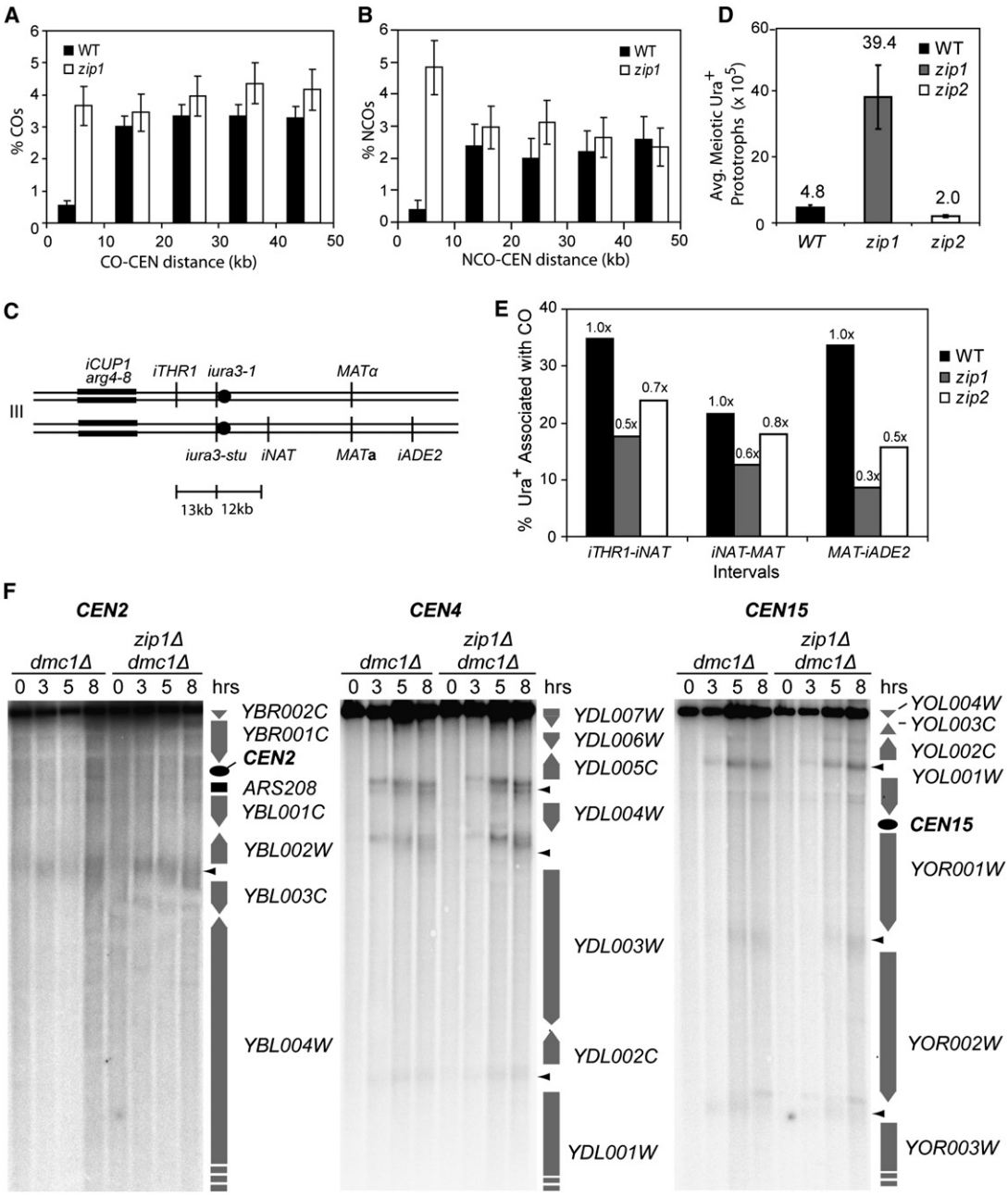

Figure 6. Centromere-Proximal CO Repression Is Relieved in a *zip1* Mutant

Comparison of centromere-proximal COs (A) and NCOs (B) in wild-type and *zip1*. (C) Chromosome III markers in a strain used to genetically measure GCs and associated crossing over at the centromere (BR4633, Rockmill et al., 2006). (D) Frequency of Ura$^+$ gene convertants from random spores of wild-type, *zip1*, and *zip2*. SDs are shown. (E) Frequency of COs associated with Ura$^+$ gene convertants for random spores of wild-type, *zip1*, and *zip2*. Fold change relative to wild-type is indicated above the bars. (F) *dmc1Δ* (NKY1455, Bishop et al. [1992]) and *dmc1Δ zip1Δ* (YAH2650, Blitzblau et al. [2007]) cells were induced to undergo meiosis, and samples were collected at the indicated time points. Genomic DNA was digested and analyzed by Southern blot. The following restriction enzymes and probes (SGD coordinates) were used: *CEN2*, SacI, II:231,552–232,350; *CEN4*, SpeI, IV:448,180–449,164; and *CEN15*, SphI/NheI, XV:331,713–332,402 (Blitzblau et al., 2007). Black arrowheads indicate major DSB sites. *CEN4* is located adjacent to *YDL001W*, off the bottom of the gel. Quantification of DSB frequencies is provided in Figure S5. Errors bars = SD.

recombination is increased at centromeres in *zip1* mutants. In comparison, no such increase was found for *zip2*. Thus, this genetic analysis concurs with our microarray analysis; moreover, it shows that the result is neither inherent to the diploid strain carrying multiple polymorphisms nor a consequence of the aberrantly high levels of recombination observed in the *zip1* tetrads used for the microarray study.

Flanking markers were used to determine whether the selected GC events are associated with crossing over (Figure 6C). In wild-type, Ura$^+$ gene convertants are associated

with crossing over 35% of the time on average (i.e., flanking marker exchange occurs in 35% of the Ura$^+$ spores) (Figure 6E). In *zip1*, only 18% on average have associated COs, consistent with the 2-fold reduction in crossing over reported in *zip1*. The frequency of crossing over also decreases in two centromere-distal intervals on chromosome III (Figure 6E), as expected for *zip1*. These results indicate that the fraction of DSB repair events resolved as COs is not increased in the centromere-adjacent interval in *zip1* and therefore cannot be responsible for the increase in centromere-proximal COs in *zip1*. This concurs with our observation from the microarray analysis that the CO:NCO ratio is unchanged.

Alternatively, more DSBs occurring in the most centromere-proximal interval could explain the increased number of COs observed in the *zip1* mutant. Contradictory to that notion, no increase in DSB hotspots is seen at the most centromere-proximal region by a genome-wide study of DSB hotspots in a *dmc1 zip1* mutant (Blitzblau et al., 2007). Three chromosomes examined by Southern analysis in a *dmc1 zip1* mutant also do not exhibit any increase in DSB activity in centromere-proximal regions as compared with the *dmc1* control (Figure 6F). Since neither a change in the CO:NCO ratio nor a change in the number of DSBs is observed, these results implicate a shift from intersister to interhomolog repair as the reason for the increase in COs at the centromere in a *zip1* mutant.

DISCUSSION

Evaluation of the Microarray Approach

The microarray-based genome-wide detection system for COs is a powerful approach for gaining information about CO control for several reasons. First, many aspects of CO behavior can be evaluated simultaneously: information about CO and GC levels, CO interference, CO homeostasis, chromatid interference, and crossing over in relationship to telomeres and centromeres can all be obtained at the same time. Second, because COs are monitored genome-wide, far fewer tetrads are needed to generate statistically significant data compared with the hundreds to thousands of tetrads needed to get similar data genetically using conventional phenotypic markers. Third, analysis of CO control is relatively rapid; data can be acquired within two weeks of making a mutant diploid strain. Finally, cell-to-cell variations can be assessed, permitting the detection of important fluctuations that would otherwise be missed in assays looking at means in large populations.

On the other hand, there are some limitations to the microarray technique. In the microarray method, only a global determination of CO control can be assessed, since the data are derived from a relatively small number of tetrads. Only with a large number of tetrads can local variations in different intervals along a chromosome or among different chromosomes be measured. In fact, local versus global observations of interference might account for differences found between genetic and microarray measurements. This could explain how *spo16* and *zip4* were observed to have normal interference in one study (Shinohara et al., 2008), but show a reduction in interference in our study. Interestingly, we do see a large local variation in interference for *spo16* in our BR1919-8B lab strain (Table S4). Completely opposing values of interference are observed in the two intervals we examined; the *HIS4-LEU2* interval shows a loss of interference (NPD = 1.3), whereas the *LEU2-MAT* interval shows normal interference (NPD = 0.35). There was no discordance in the one common interval between our study and that of Shinohara; both studies report normal interference in the *LEU2-MAT* interval. Another example whose local versus global evaluations might differ is *ndj1*, which was shown previously to have somewhat impaired interference (Chua and Roeder, 1997), but exhibits normal interference in our genomic analysis. One possibility for the difference in interference seen in *ndj1* is the potential variation in interference between small and large chromosomes, since the genetic study was carried out on only one small chromosome (III). Local variations might also account for the negative interference of *zip4* rather than the existence of a subpopulation, since technically, there is no statistically significant difference between 1 outlier in 34 tetrads (*zip4*) and zero outliers in 26 tetrads (wild-type or *zip2*).

zip2 and zip4 Affect CO Homeostasis

Analysis of a series of *SPO11* alleles with decreasing frequencies of DSBs revealed the existence of CO homeostasis in an otherwise wild-type strain (Martini et al., 2006). Our observation that wild-type shows no correlation between COs and NCOs confirms that CO homeostasis is part of normal CO control. It has been proposed that the molecular mechanism that gives rise to CO interference may also be responsible for CO homeostasis (Martini et al., 2006). This hypothesis predicts that any observed loss of interference would be accompanied by a concomitant loss of homeostasis. Supporting this notion, we see a reduction of CO homeostasis in two mutants (*zip2* and *zip4*) that show reduced interference. However, although interference was almost completely abolished in these mutants, the reduction of CO homeostasis was more modest, suggesting that the connection between CO homeostasis and interference is more complex.

CO Prevention at the Centromere

Centromere-proximal crossing over contributes to aneuploidy in budding yeast due to precocious separation of sister chromatids (PSSC) at meiosis I (Rockmill et al., 2006). In *Drosophila* and humans, COs near the centromere also predispose a chromosome to segregate aberrantly (Hassold and Hunt, 2001; Koehler et al., 1996a), suggesting that prevention of COs near centromeres may be critical for the proper alignment of homologs. Our finding that centromeric repression of crossing over depends on Zip1 is consistent with the timing and localization of Zip1 on meiotic chromosomes. Tsubouchi and Roeder (2005) showed that Zip1 holds chromosomes together in pairs at their centromeres, early in meiotic prophase when the homology search is underway. Early in prophase I, many nonhomologous centromere couplings are found, but these decrease as chromosomes find their correct partners. Important to the homology search is DSB formation by the Spo11 protein, resulting in strand invasion reactions that likely stabilize and define a homologous pair. Because centromere coupling initially takes place between nonhomologous centromeres, there may be a need to suppress homology assessment at centromeres. The Zip1-dependent bias toward intersister versus interhomolog recombination near centromeres may act to limit homology searches nearby and promote searches in more distal regions.

Microarray Mapping of COs and NCOs

Recently, a similar method using tiling arrays with a median distance of 78 bp between consecutive markers was used to map meiotic COs and NCOs in wild-type and *msh4* for the same S96/YJM789 hybrid used in our study (Mancera et al., 2008). In agreement with our analyses, their study reports that wild-type strains show interference and *msh4* strains have lost interference. Particularly noteworthy is that the higher resolution of their study permitted a better analysis of the relationship between COs and NCOs and a more accurate assessment of NCO tract lengths and frequencies. The high-resolution CO and NCO maps revealed the existence of genomic locations with distinct preferences for COs or NCOs. Although we are limited in our ability to detect GCs, our observation that GC_{CO}s have larger tract lengths than NCOs is confirmed by their study. Our in-depth analyses of CO control in wild-type and several mutants and our extensive analysis of telomeres and centromeres, together with the high-resolution analysis of NCOs of Mancera et al. (2008), clearly demonstrate the power of this microarray-based approach and utility in future studies of meiotic recombination.

EXPERIMENTAL PROCEDURES

Strains

Haploid yeast strains S96 and YJM789 were used in this study (Winzeler et al., 1998). Deletion strains were constructed by PCR-mediated gene replacement using the pFA6a-kanMX6 plasmid as the template (Longtine et al., 1998). Genotypes of strains are listed in Table S9. In all but *zip1*, haploid strains were mated and zygotes were picked after 4 hr and allowed to grow on YPAD plates for <3 days to minimize mismatch repair before being transferred to 2% potassium acetate sporulation plates at 30°C. Tetrads were dissected after 3–5 days. For *zip1*, because the sporulation of four-spore tetrads was so low, zygotes were taken en masse and patched to a sporulation plate after 6–8 hr of mating.

Southern Analysis

To induce synchronous meiosis, strains were preinoculated at OD_{600} = 0.3 in BYTA medium (50 mM potassium phthalate, 1% yeast extract, 2% bactotryptone, 1% potassium acetate), grown for 16 hr at 30°C, washed twice, and resuspended at OD_{600} = 1.9 in SPO medium (0.3% potassium acetate). Southern analysis was performed as described by Blitzblau et al. (2007).

Sample Preparation

Genomic DNA was purified from 100 ml of overnight YPAD culture using a QIAGEN genomic-tip 500/G following the QIAGEN genomic DNA handbook with the slight modification of extending zymolyase and protease K digestion to 1 hr. Fifteen micrograms of genomic DNA was digested into 50- to 100-bp fragments and end-labeled as previously described (Winzeler et al., 2003). Labeled DNA fragments were then hybridized to Affymetrix Yeast Genome S98 arrays (Gladstone Institute, San Francisco, CA).

Data Analysis

Marker designations and CO locations were determined using the Allelescan software. In our CrossOver software, programs were written to generate the distributions for our analysis using the output segregation file from Allelescan. Analyses of chromatid interference and GC_{CO}s and NCOs are part of the CrossOver software. A description of the interference analysis and the simulation algorithm is provided in Supplemental Experimental Procedures.

Genetics

Genetic analyses of *zip1* near the centromere were carried out as described by Rockmill et al. (2006).

Correlation Coefficient Analysis

Using the inherent DSB fluctuation expected on a cell-to-cell basis, we assayed the intensity of the association between COs and NCOs to assess what might be homeostatically controlled. CO homeostasis was measured by a lack of statistical association between fluctuations in CO number and NCO number. We quantified the extent of statistical association between the two numbers using the Pearson's correlation coefficient, a measure of statistical association between two random variables that generates values in the range of −1.0 to 1.0. Statistical significance between the mutant and wild-type was determined using an analysis comparing a control correlation coefficient to each other mutant correlation coefficient (Zar, 1984). If the control set of data is B and each other group of data is A, we can compute $q = (z_B - z_A)/SE$, where $z = 0.5 * \ln([1 + r]/[1 - r])$, r is the correlation coefficient, and $SE = \mathrm{sqrt}(1/[n_A - 3] + 1/[n_B - 3])$ in the case where sample sizes (n_A and n_B) are not the same. The critical value for the q statistic is given in Figure 5C. Below, examples are provided for the various potential relationships between COs and NCOs in the face of fluctuating DSBs.

Positive Correlation Coefficient: Fixed CO:NCO Ratio

In the case of a fixed CO:NCO ratio, cells with lower numbers of DSBs would be expected to show correspondingly low numbers of NCOs and COs, and cells with higher numbers of DSBs would be expected to show correspondingly high numbers of NCOs and COs, thus giving a positive correlation coefficient.

Negative Correlation Coefficient: Fixed CO + NCO

A negative correlation coefficient would be indicative of maintenance of the overall total of NCOs and COs such that an increase in one comes at the expense of the other. This would be expected if the number of DSBs did not vary between cells, but instead, the CO:NCO ratio was variable.

Zero Correlation Coefficient: CO Level Maintained or NCO Level Maintained

A correlation coefficient of zero can have either of two meanings. It could mean that the two variables that are being tested for correlation have absolutely nothing to do with each other. Alternatively, if there is a known relationship expected between two variables that is established by other data, it could mean that one variable is being controlled (homeostasis) and the other variable is not. In the case of COs and NCOs, the fact that both are derived from DSBs rules out the possibility that COs and NCOs have nothing to do with each other. A zero correlation coefficient could therefore mean that either the CO level is homeostatically controlled or the NCO level is homeostatically controlled. Since the coefficient of variation (CV = SD/mean) for NCOs is larger than that for COs (CV_{NCO} = 0.45 versus CV_{CO} = 0.10), it suggests that homeostatic control is exerted on the COs.

ACCESSION NUMBERS

The GEO accession number for the arrays outlined here is GSE12170.

SUPPLEMENTAL DATA

The Supplemental Data for this article include five figures, nine tables, Supplemental Results, Supplemental Experimental Procedures, and Supplemental References, and are available online at http://www.developmentalcell.com/cgi/content/full/15/3/401/DC1/.

ACKNOWLEDGMENTS

We give thanks to Amy MacQueen and Wallace Marshall for critical reading of the manuscript. We also thank Wallace Marshall and Tetsuya Matsuguchi for technical and programming advice. S.C is supported by a Genentech Fellowship. J.F is supported by the American Cancer Society Research Scholar Award (RSG CCG 110688) and the UCSF Sandler Fellows Program.

Received: February 19, 2008
Revised: June 5, 2008
Accepted: July 18, 2008
Published online: August 7, 2008

REFERENCES

Agarwal, S., and Roeder, G.S. (2000). Zip3 provides a link between recombination enzymes and synaptonemal complex proteins. Cell *102*, 245–255.

Barton, A.B., Pekosz, M., Kurvathi, R.S., and Kaback, D.B. (2008). Meiotic recombination at chromosome ends in *Saccharomyces cerevisiae*. Genetics, in press. Published online June 18, 2008. 10.1534/genetics.107.083493.

Baudat, F., and de Massy, B. (2007). Regulating double-stranded DNA break repair towards crossover or non-crossover during mammalian meiosis. Chromosome Res. *15*, 565–577.

Bishop, D.K., Park, D., Xu, L., and Kleckner, N. (1992). *DMC1*: a meiosis-specific yeast homolog of E. coli *recA* required for recombination, synaptonemal complex formation, and cell cycle progression. Cell *69*, 439–456.

Blitzblau, H.G., Bell, G.W., Rodriguez, J., Bell, S.P., and Hochwagen, A. (2007). Mapping of meiotic single-stranded DNA reveals double-stranded-break hotspots near centromeres and telomeres. Curr. Biol. *17*, 2003–2012.

Borts, R.H., and Haber, J.E. (1987). Meiotic recombination in yeast: alteration by multiple heterozygosities. Science *237*, 1459–1465.

Broman, K.W., Rowe, L.B., Churchill, G.A., and Paigen, K. (2002). Crossover interference in the mouse. Genetics *160*, 1123–1131.

Buhler, C., Borde, V., and Lichten, M. (2007). Mapping meiotic single-strand DNA reveals a new landscape of DNA double-strand breaks in *Saccharomyces cerevisiae*. PLoS Biol. *5*, e324.

Carpenter, A.T.C. (1988). Thoughts on recombination nodules, meiotic recombination, and chiasmata. In Genetic Recombination, R. Kucherlapati and G.R. Smith, eds. (Washington, D.C.: American Society for Microbiology), pp. 529–548.

Cherry, J.M., Ball, C., Weng, S., Juvik, G., Schmidt, R., Adler, C., Dunn, B., Dwight, S., and Riles, L. (1997). Genetic and physical maps of *Saccharomyces cerevisiae*. Nature ***387***(6632, Suppl), 67–73.

Chua, P.R., and Roeder, G.S. (1997). Tam1, a telomere-associated meiotic protein, functions in chromosome synapsis and crossover interference. Genes Dev. *11*, 1786–1800.

Chua, P.R., and Roeder, G.S. (1998). Zip2, a meiosis-specific protein required for the initiation of chromosome synapsis. Cell *93*, 349–359.

Copenhaver, G.P., Housworth, E.A., and Stahl, F.W. (2002). Crossover interference in *Arabidopsis*. Genetics *160*, 1631–1639.

de Boer, E., Stam, P., Dietrich, A.J., Pastink, A., and Heyting, C. (2006). Two levels of interference in mouse meiotic recombination. Proc. Natl. Acad. Sci. USA *103*, 9607–9612.

Fogel, S., Mortimer, R., Lusnak, K., and Tavares, F. (1978). Meiotic gene conversion: a signal of the basic recombination event in yeast. Cold Spring Harb. Symp. Quant. Biol. *43*, 1325–1341.

Foss, E.J., and Stahl, F.W. (1995). A test of a counting model for chiasma interference. Genetics *139*, 1201–1209.

Fung, J.C., Rockmill, B., Odell, M., and Roeder, G.S. (2004). Imposition of crossover interference through the nonrandom distribution of synapsis initiation complexes. Cell *116*, 795–802.

Guillon, H., Baudat, F., Grey, C., Liskay, R.M., and de Massy, B. (2005). Crossover and noncrossover pathways in mouse meiosis. Mol. Cell *20*, 563–573.

Hassold, T., and Hunt, P. (2001). To err (meiotically) is human: the genesis of human aneuploidy. Nat. Rev. Genet. *2*, 280–291.

Hassold, T.H., Abruzzo, M., Adkins, K., Griffin, D., Merrill, M., Millie, E., Saker, D., Shen, J., and Zaragoza, M. (1996). Human aneuploidy: Incidence, origin, and etiology. Environ. Mol. Mutagen. *28*, 167–175.

Hassold, T., Hall, H., and Hunt, P. (2007). The origin of human aneuploidy: where we have been, where we are going. Hum. Mol. Genet. *16*, 203–208.

Hillers, K.J. (2004). Crossover interference. Curr. Biol. *14*, R1036–R1037.

Huitema, B.E. (1974). Three multiple comparison procedures for contrasts among correlation coefficients. Proc. Soc. Statist. *1974*, 336–339.

Jeffreys, A.J., and May, C.A. (2004). Intense and highly localized gene conversion activity in human meiotic crossover hot spots. Nat. Genet. *36*, 151–156.

Jones, G.H. (1984). The control of chiasma distribution. Symp. Soc. Exp. Biol. *38*, 293–320.

Kaback, D.B., Guacci, V., Barber, D., and Mahon, J.W. (1992). Chromosome size-dependent control of meiotic recombination. Science *256*, 228–232.

Keeney, S., Giroux, C.N., and Kleckner, N. (1997). Meiosis-specific DNA double-strand breaks are catalyzed by Spo11, a member of a widely conserved protein family. Cell *88*, 375–384.

Koehler, K.E., Boulton, C.L., Collins, H.E., French, R.L., Herman, K.C., Lacefield, S.M., Madden, L.D., Schuetz, C.D., and Hawley, R.S. (1996a). Spontaneous X chromosome MI and MII nondisjunction events in *Drosophila melanogaster* oocytes have different recombinational histories. Nat. Genet. *14*, 406–414.

Koehler, K.E., Hawley, R.S., Sherman, S., and Hassold, T. (1996b). Recombination and nondisjunction in humans and flies. Hum. Mol. Genet. *5*, 1495–1504.

Lacefield, S., and Murray, A.W. (2007). The spindle checkpoint rescues the meiotic segregation of chromosomes whose crossovers are far from the centromere. Nat. Genet. *39*, 1273–1277.

Lamb, N.E., Freeman, S.B., Savage-Austin, A., Pettay, D., Taft, L., Hersey, J., Gu, Y., Shen, J., Saker, D., May, K.M., et al. (1996). Susceptible chiasmate configurations of chromosome 21 predispose to non-disjunction in both maternal meiosis I and meiosis II. Nat. Genet. *14*, 400–405.

Lambie, E.J., and Roeder, G.S. (1986). Repression of meiotic crossing over by a centromere (CEN3) in *Saccharomyces cerevisiae*. Genetics *114*, 769–789.

Lambie, E.J., and Roeder, G.S. (1988). A yeast centromere acts in cis to inhibit meiotic gene conversion of adjacent sequences. Cell *52*, 863–873.

Levy, K.J. (1979). Pairwise comparisons associated with the K independent sample median test. Am. Stat. *33*, 138–139.

Longtine, M.S., McKenzie, A., III, Demarini, D.J., Shah, N.G., Wach, A., Brachat, A., Phillippsen, P., and Pringle, J.R. (1998). Additional modules for versatile and economical PCR-based gene deletion and modification in *Saccharomyces cerevisiae*. Yeast *14*, 953–961.

Lynn, A., Soucek, R., and Borner, G.V. (2007). ZMM proteins during meiosis: crossover artists at work. Chromosome Res. *15*, 591–605.

Malkova, A., Swanson, J., German, M., McCusker, J.H., Housworth, E.A., Stahl, F.W., and Haber, J.E. (2004). Gene conversion and crossing over along the 405-kb left arm of *Saccharomyces cerevisiae* chromosome VII. Genetics *168*, 49–63.

Mancera, E., Bourgon, R., Brozzi, A., Huber, W., and Steinmetz, L.M. (2008). High-resolution mapping of meiotic crossovers and non-crossovers in yeast. Nature in press. Published online July 9, 2008. 10.1038/nature07135.

Martini, E., Diaz, R.L., Hunter, N., and Keeney, S. (2006). Crossover homeostasis in yeast meiosis. Cell *126*, 285–295.

McPeek, M.S., and Speed, T.P. (1995). Modeling interference in genetic recombination. Genetics *139*, 1031–1044.

Mortimer, R., and Fogel, S. (1974). Genetical interference and gene conversion. In Mechanisms in Recombination, R. Grell, ed. (New York: Plenum Press), pp. 263–275.

Muller, H. (1916). The mechanism of crossing over. Am. Nat. *50*, 193–221.

Novak, J.E., Ross-Macdonald, P., and Roeder, G.S. (2001). The budding yeast Msh4 protein functions in chromosome synapsis and the regulation of crossover distribution. Genetics *158*, 1013–1025.

Ott, J. (1991). Analysis of Human Genetic Linkage (Baltimore: Johns Hopkins University Press).

Papazian, H.P. (1952). The analysis of tetrad data. Genetics *37*, 175–188.

Perkins, D.D. (1962). Crossing-over and interference in a multiply marked chromosome arm of *Neurospora*. Genetics *47*, 1253–1274.

Petes, T.D. (2001). Meiotic recombination hot spots and cold spots. Nat. Rev. Genet. *2*, 360–369.

Rockmill, B., Fung, J.C., Branda, S.S., and Roeder, G.S. (2003). The Sgs1 helicase regulates chromosome synapsis and meiotic crossing over. Curr. Biol. *13*, 1954–1962.

Rockmill, B., Voelkel-Meiman, K., and Roeder, G.S. (2006). Centromere-proximal crossovers are associated with precocious separation of sister chromatids during meiosis in *Saccharomyces cerevisiae*. Genetics *174*, 1745–1754.

Roeder, G.S. (1997). Meiotic chromosomes: it takes two to tango. Genes Dev. *11*, 2600–2621.

Sall, T., and Bengtsson, B.O. (1989). Apparent negative interference due to variation in recombination frequencies. Genetics *122*, 935–942.

Shinohara, M., Oh, S.D., Hunter, N., and Shinohara, A. (2008). Crossover assurance and crossover interference are distinctly regulated by the ZMM proteins during yeast meiosis. Nat. Genet. *40*, 299–309.

Storlazzi, A., Xu, L., Schwacha, A., and Kleckner, N. (1996). Synaptonemal complex (SC) component Zip1 plays a role in meiotic recombination independent of SC polymerization along the chromosomes. Proc. Natl. Acad. Sci. USA *93*, 9043–9048.

Su, Y., Barton, A.B., and Kaback, D.B. (2000). Decreased meiotic reciprocal recombination in subtelomeric regions in *Saccharomyces cerevisiae*. Chromosoma *109*, 467–475.

Sym, M., and Roeder, G.S. (1994). Crossover interference is abolished in the absence of a synaptonemal complex protein. Cell *79*, 283–292.

Sym, M., Engebrecht, J., and Roeder, G.S. (1993). ZIP1 is a synaptonemal complex protein required for meiotic chromosome synapsis. Cell *72*, 365–378.

Tsubouchi, T., and Roeder, G.S. (2005). A synaptonemal complex protein promotes homology-independent centromere coupling. Science *308*, 870–873.

Tsubouchi, T., Zhao, H., and Roeder, G.S. (2006). The meiosis-specific Zip4 protein regulates crossover distribution by promoting synaptonemal complex formation together with Zip2. Dev. Cell *10*, 809–819.

Wei, W., McCusker, J.H., Hyman, R.W., Jones, T., Ning, Y., Cao, Z., Gu, Z., Bruno, D., Miranda, M., Nguyen, M., et al. (2007). Genome sequencing and comparative analysis of *Saccharomyces cerevisiae* strain YJM789. Proc. Natl. Acad. Sci. USA *104*, 12825–12830.

Winzeler, E.A., Richards, D.R., Conway, A.R., Goldstein, A.L., Kalman, S., McCullough, M.J., McCusker, J.H., Stevens, D.A., Wodicka, L., Lockhart, D.J., et al. (1998). Direct allelic variation scanning of the yeast genome. Science *281*, 1194–1197.

Winzeler, E.A., Castillo-Davis, C.I., Oshiro, G., Liang, D., Richards, D.R., Zhou, Y., and Hartl, D.L. (2003). Genetic diversity in yeast assessed with whole-genome oligonucleotide arrays. Genetics *163*, 79–89.

Wu, H.Y., and Burgess, S.M. (2006). Ndj1, a telomere-associated protein, promotes meiotic recombination in budding yeast. Mol. Cell. Biol. *26*, 3683–3694.

Zar, J. (1984). Biostatistical Analysis, Second Edition (Upper Saddle River: Prentice Hall).

Zhao, H., Speed, T.P., and McPeek, M.S. (1995). Statistical analysis of crossover interference using the chi-square model. Genetics *139*, 1045–1056.

Zickler, D., and Kleckner, N. (1999). Meiotic chromosomes: integrating structure and function. Annu. Rev. Genet. *33*, 603–754.